

# Element-specific field-induced spin reorientation and an unusual tetracritical point in $\text{MnCr}_2\text{S}_4$

Sh. Yamamoto,<sup>1,\*</sup> H. Suwa,<sup>2</sup> T. Kihara,<sup>3</sup> T. Nomura,<sup>1,4</sup> Y. Kotani,<sup>5</sup> T. Nakamura,<sup>3,5</sup> Y. Skourski,<sup>1</sup> S. Zherlitsyn,<sup>1</sup> L. Prodan,<sup>6,7</sup> V. Tsurkan,<sup>6,7</sup> H. Nojiri,<sup>3</sup> A. Loidl,<sup>7</sup> and J. Wosnitza<sup>1,8</sup>

<sup>1</sup>*Hochfeld-Magnetlabor Dresden (HLD-EMFL) and Würzburg-Dresden Cluster of Excellence ct.qmat, Helmholtz-Zentrum Dresden-Rossendorf, 01328 Dresden, Germany*

<sup>2</sup>*Department of Physics, The University of Tokyo, Tokyo 113-0033, Japan*

<sup>3</sup>*Institute for Materials Research, Tohoku University, Sendai 980-8577, Japan*

<sup>4</sup>*Institute for Solid State Physics, The University of Tokyo, Kashiwa, Chiba 277-8581, Japan*

<sup>5</sup>*Japan Synchrotron Radiation Research Institute, SPring-8, Sayo, Hyogo 679-5198, Japan*

<sup>6</sup>*Institute of Applied Physics, MD 2028, Chisinau, R. Moldova*

<sup>7</sup>*Experimental Physics 5, Center for Electronic Correlations and Magnetism, Institute of Physics, University of Augsburg, 86159, Augsburg, Germany*

<sup>8</sup>*Institut für Festkörper- und Materialphysik, TU Dresden, 01062 Dresden, Germany*

(Dated: September 1, 2020)

The ferrimagnetic spinel  $\text{MnCr}_2\text{S}_4$  shows a variety of magnetic-field-induced phase transitions owing to bond frustration and strong spin-lattice coupling. However, the site-resolved magnetic properties at the respective field-induced phases in high magnetic fields remain elusive. Our soft x-ray magnetic circular dichroism studies up to 40 T directly evidence element-selective magnetic-moment reorientations in the field-induced phases. The complex magnetic structures are further supported by entropy changes extracted from magnetocaloric-effect measurements. Moreover, thermodynamic experiments reveal an unusual tetracritical point in the  $H$ - $T$  phase diagram of  $\text{MnCr}_2\text{S}_4$  due to strong spin-lattice coupling.

Frustrated magnets with competing magnetic interactions offer an exceptional playground for studying a variety of exotic magnetic states and emergent magnetic excitations [1]. The competing interactions between the constituent magnetic ions can be fine-tuned by applying an external magnetic field, which stabilizes various field-induced states with complex magnetic structures [2, 3]. This leads to a rich magnetic-field-temperature ( $H$ - $T$ ) phase diagram that also can be used as a test bed for validating various theoretical models [4, 5]. Cubic spinels  $AB_2X_4$ , where  $A$  and  $B$  represent magnetic cations, belong to paradigmatic frustrated systems. Geometrical frustration results from the  $B$  magnetic cation being located at the vertices of a pyrochlore lattice with antiferromagnetic (AFM) exchange interactions, whereas bond frustration is caused by the competing exchange interactions of  $J_{A-A}$ ,  $J_{A-B}$ , and  $J_{B-B}$  [6]. In addition to the magnetic frustration, a strong spin-lattice coupling gives rise to a robust magnetization plateau, to unconventional metastable magnetostructural [7], and to spin-driven multiferroic states [8].

$\text{MnCr}_2\text{S}_4$  crystallizes in a normal cubic-type spinel structure (space group  $Fd\bar{3}m$ ) where the  $\text{Mn}^{2+}$  ( $S = 5/2$ ,  $3d^5$ ) and  $\text{Cr}^{3+}$  ( $S = 3/2$ ,  $3d^3$ ) ions reside on the tetrahedral  $A$  and octahedral  $B$  sites, respectively. This results in a bond frustration with competing AFM interactions between  $J_{\text{Mn-Cr}}$  and  $J_{\text{Mn-Mn}}$ . The title compound shows two consecutive transitions at  $T_C \approx 65$  K to a ferrimagnetic state and at  $T_{\text{YK}} \approx 5$  K to a canted spin configuration [9]. It is suggested that at  $T_{\text{YK}}$ , the Yafet-Kittel (YK) phase is stabilized. This phase is composed of two nonequivalent manganese sites, Mn1 and Mn2, with the magnetic moments rotated by  $+120^\circ$  and  $-120^\circ$  with respect to

the chromium moment that is parallel to the external magnetic field caused by the strong  $J_{\text{Cr-Cr}}$  FM interaction [10]. A variety of magneto-structural phases have been identified in the  $H$ - $T$  phase diagram spanning up to 100 T and below 20 K, including a robust plateau between 25-50 T [11] (see Sec. I of the Supplemental Material [12]). In addition, from a quantum lattice-gas model, the YK state and the intermediate phase, which is located between the YK and plateau phases, were suggested to be spin-superfluid and spin-supersolid states, respectively [13–15]. Very recently, multiferroicity has been reported in the YK and intermediate phases of  $\text{MnCr}_2\text{S}_4$  [16, 17]. However, a detailed understanding of the magnetic structure in the field-induced phases in  $\text{MnCr}_2\text{S}_4$  is still missing. Magnetic spinels with a single magnetic ion could be studied in details by use of bulk magnetization and neutron scattering measurements [18, 19].  $\text{MnCr}_2\text{S}_4$ , however, possesses two magnetic ions featured by the site-specific magnetic properties at the  $A$  and  $B$  sites. This makes bulk-magnetization studies quite challenging to reveal the microscopic nature of the field-induced phases.

In this work, we investigate the microscopic nature by performing soft x-ray magnetic circular dichroism (XMCD) measurements of a  $\text{MnCr}_2\text{S}_4$  single crystal in pulsed magnetic fields along with macroscopic thermodynamic experiments. The element-selective XMCD study, complemented by the extracted entropy changes, reveals a complex sublattice-moment rotation at the manganese and chromium sites in fields up to 40 T. Furthermore, the observed magnetocaloric effect (MCE) together with ultrasound and specific-heat measurements reveal a tetracritical point (TP) owing to spin-lattice coupling in the  $H$ - $T$

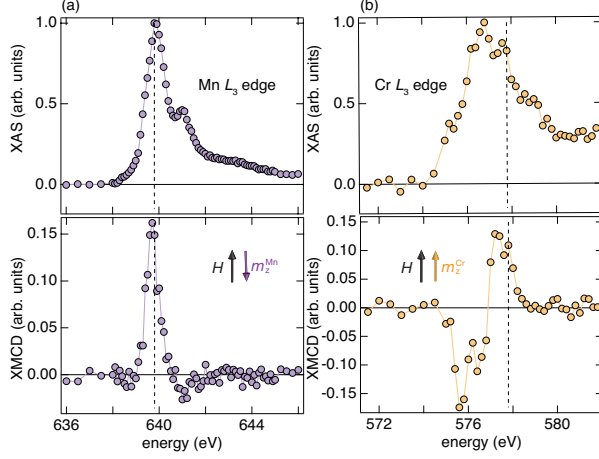


FIG. 1: XAS and XMCD spectra for the (a) Mn and (b) Cr  $L_3$  edge. These spectra were obtained in zero field at 15 K after a field pulse of 20 T was applied along the [110] axis to induce a single-magnetic domain state. The vertical dashed lines represent the photon energies at which magnetic-field-dependent XMCD data were recorded [Figs. 2(b) and 3]. The spectra are normalized to the  $L_3$  XAS peak intensity. The illustration shows the relation of the longitudinal sublattice magnetization,  $m_z$ , with respect to the initial-field direction,  $H$ , (see text for details).

phase diagram, which is a rather surprising finding in an isotropic Heisenberg magnet.

We performed various experiments including soft XMCD at the Mn and Cr  $L_3$  edges as well as magnetocaloric effect complemented by specific-heat and ultrasound experiments. Details of the experimental methods are described in Sec. II of the Supplemental Material [12]. We note the very weak magnetic anisotropy due to half-filled  $e_g$  and  $t_{2g}$  ( $\text{Mn}^{2+}$ ) and  $t_{2g}$  ( $\text{Cr}^{3+}$ ) states with zero orbital moment. Thus ensures that the present results in high magnetic fields are independent on the field direction. This was verified in previous studies that showed no magnetic anisotropy above 0.5 T [9, 20].

Figure 1 shows zero-field X-ray absorption spectroscopy (XAS) and XMCD results at the Mn and Cr  $L_3$  edge measured at 15 K. In order to prepare a single-magnetic domain, a pulsed field of up to 20 T along the [110] axis (hereafter called initial field) was applied before taking the zero-field spectra. The XAS spectra with multiplet structures agree with those previously reported for  $\text{Mn}^{2+}$  in tetrahedral [21] and  $\text{Cr}^{3+}$  in octahedral symmetry [22, 23]. Note that the Mn XAS and XMCD give an average information on the two nonequivalent Mn sublattices. The largest XMCD features near the  $L_3$  edge (Mn at  $\sim 639.8$  eV and Cr at  $\sim 576$  eV) show an opposite sign of the XMCD amplitude, documenting the antiparallel coupling between the Mn and Cr  $3d$  longitudinal moments ( $m_z$ ). In static-field bulk magnetization measurements, no remanence has been observed at tem-

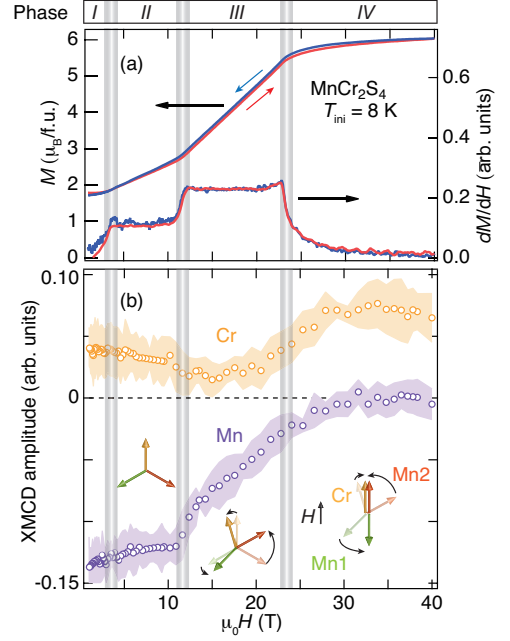


FIG. 2: (a) Field dependence of the bulk magnetization (left scale) and its field derivative (right scale). (b) Mn (purple) and Cr (orange) XMCD amplitudes are shown by symbols as function of magnetic field. The sign of the Mn XMCD is reversed for correspondence to the relative Mn sublattice magnetization. The shaded areas indicate the experimental errors. All data were collected at the initial temperature of 8 K. The vertical lines separate the phases I-IV, which are indicated on top of the figure. Schematic diagrams of the spin structures at the respective phase II, III, and IV are illustrated with orange for Cr, and green (red) arrows for Mn1 (Mn2). See text for details.

peratures above 5 K [9]. The zero-field XMCD results imply that finite moments of the Mn and Cr sublattice are oriented antiparallel to each other in the initial-field axis, with the net moment is zero. The dashed line in Fig. 1(a) [Fig. 1(b)] indicates the photon energy of 639.8 eV (577.8 eV), which was chosen for studying the Mn (Cr) sublattice magnetization in pulsed-field XMCD experiments shown in Figs. 2(b) and 3. The positive XMCD amplitude at these photon energies corresponds to the (anti)parallel Cr (Mn)  $3d$  magnetic moment  $m_z^{\text{Cr}}$  ( $m_z^{\text{Mn}}$ ) with respect to the field direction.

Figures 2(a) and 2(b) show bulk magnetization data and element-selective  $L_3$ -edge XMCD up to 40 T, respectively, recorded at the initial temperature  $T_{\text{ini}}$  of 8 K in pulsed magnetic fields. The XMCD amplitude is proportional to the total moment ( $m_z$ ) of the respective atom [24, 25]. The sign of the Mn XMCD amplitude at 639.8 eV is reversed to provide correspondence with the direction of the moment of the Mn sublattice with respect to the field direction as shown in the illustration of Fig. 1 and which is also valid for Fig. 3. The bulk magnetization and its field derivative signal a sequence of successive phase tran-

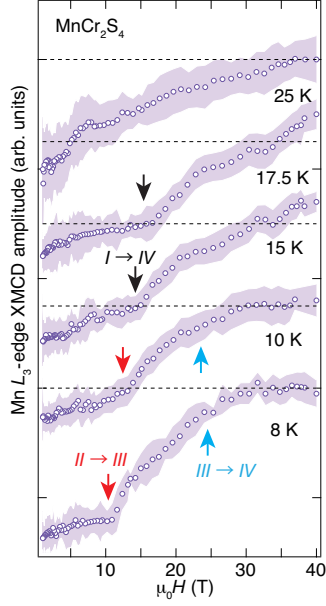


FIG. 3: Field dependence of the Mn  $L_3$ -edge XMCD amplitude with the experimental errors shown by the shaded area at selected initial temperatures  $T_{\text{ini}}$ . The sign of the XMCD amplitudes is inverted to provide correspondence with the relative Mn sublattice magnetization. The data for  $T_{\text{ini}} = 8$  K are the same as that shown in Fig. 2(b). The results for the field scans between 10 and 25 K are vertically shifted for clarity. The horizontal dashed lines show the zero level, which is close to the maximum field at each temperature. The red, blue, and black arrows denote the anomalies, which signal the phase transitions of  $II \rightarrow III$ ,  $III \rightarrow IV$ , and  $I \rightarrow IV$ , respectively.

sitions ranging from  $I$  to  $IV$  as shown at the top of Fig. 2. These phases are suggested to be  $I$  (ferrimagnetic order with disordered transverse components of the moments of the Mn ions),  $II$  (YK state),  $III$  (low-field asymmetric state), and  $IV$  (plateau state) [15].

In Ref. [15], the low-field asymmetric state was described by a spin configuration with a tilted triangular structure, when compared to the YK configuration, however, with the chromium moments still aligned strictly parallel to the external magnetic field. In earlier work, this asymmetric spin state was thought to result from the manganese spins located at the two nonequivalent tetrahedral sites bearing magnetic moments of different length and sign [26] or this spin state was described by an “oblique” spin configuration with deviations of the chromium moments from the external field direction, a configuration which was thought to be stabilized by bi-quadratic exchange [27]. Similar spin structures, with the chromium moments not parallel to the external field were proposed and were shown to result from strong spin-lattice coupling effects [11].

Figure 2(b) shows that the Cr and Mn XMCD amplitudes remain almost constant in phase  $I$  and  $II$ . The Mn XMCD amplitude markedly starts to

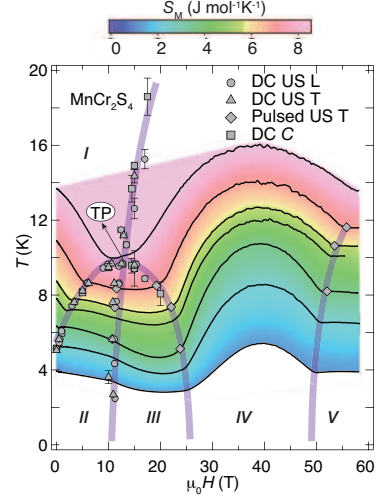


FIG. 4: Color-coded magnetic entropy  $S_M$  in the  $H$ - $T$  plane, extracted from isentropic temperature variations in magnetic field shown by the black solid lines. The phase boundaries as determined by static (DC) and pulsed-field ultrasound (US) experiments for longitudinal (L) and transverse (T) acoustic modes, as well as from specific-heat (C) experiments are shown by symbols. The purple lines are guides to the eye and separate the phases  $I$ - $V$ .

increase above  $\sim 11.5$  T in phase  $III$ , which reflects the simultaneous rotation of the Mn1 and Mn2 moments and indicate a continuous increase of the opening angle between Mn1 and Mn2 moments. This finally leads to the collinear AFM state of the Mn1 and Mn2 spins along the field direction  $[110]$  in phase  $IV$  where the Mn XMCD amplitude becomes zero. On the other hand, the Cr XMCD amplitude decreases slightly in phase  $III$  (Fig. 2). This could indeed reflect the deviation of the Cr magnetic moments from the original direction parallel to the field in the phase  $II$ , which was predicted in a recent study and was explained by strong spin-lattice coupling [11]. In phase  $IV$ , the Cr XMCD amplitude further increases and reaches its saturation significantly larger than the amplitude in phase  $II$ . The magnetic structures deduced from the XMCD data are shown in Fig. 2(b), which provides element-selective information on the proposed YK ( $II$ ), low-field asymmetric ( $III$ ), and plateau ( $IV$ ) states. As discussed in the following, this microscopic picture is further supported by our pulsed-field MCE measurements (Fig. 4).

In the temperature range below 20 K, the moment of the Mn sublattice is anticipated to be responsible for the main contributions to the field-induced changes in the bulk magnetization, rather than the Cr counterpart [9]. Figure 3 shows the field dependence of the Mn  $L_3$ -edge XMCD amplitude at selected  $T_{\text{ini}}$ . At  $T_{\text{ini}} = 8$  and 10 K, the system evolves through the phases  $I$ ,  $II$ ,  $III$ , and  $IV$  as shown in Fig. 4. The field-dependent XMCD amplitude signals the transitions of  $II \rightarrow III$  and  $III \rightarrow IV$ . At  $T_{\text{ini}} = 15$  and

17.5 K, anomalies are identified that correspond to the phase transition from *I* to *IV*. At  $T_{\text{ini}} = 25$  K, no anomaly is detected up to 40 T, which well agrees with the previous magnetization data [15]. We note that Monte Carlo simulation suggests subtle displacements of the sulfur atoms that bridge the Mn and Cr cations [11]. In future, it will be important to investigate the lineshapes of XAS/XMCD spectra at high magnetic fields in phase *III* and *IV*, which could provide further insights into such subtle changes of the local environments.

Now, we present the thermodynamic results. Figure 4 shows the contour plot of the magnetic entropy  $S_M$  extracted from the isentropic  $T(H)$  data (black solid lines) obtained in pulsed fields up to 60 T. The phase boundaries are drawn by purple lines deduced from ultrasound and specific-heat anomalies (see Sec. III of the Supplemental Material [12]), which separate the phases *I*-*V* (see Sec. I of the Supplemental Material [12]). The absolute values of the entropy were calibrated with data at 10 T from literature [9].

Each MCE trace shows multiple kinks that signal successive magnetic phase transitions. Obviously, the MCE exhibits the anomalies at the same positions as those deduced from ultrasound and specific-heat measurements. Starting from the phase *I*, the temperature decreases in the adiabatic processes due to the increase of  $S_M$  toward the phases *II* and *III*. After entering the phase *IV*, the adiabatic temperature remarkably increases resulting from the decrease of  $S_M$  up to 40 T. Then  $S_M$  increases toward the phase *V* and levels off. The overall phase boundaries are qualitatively in good agreement with the previous works based on other macroscopic experiments [11, 15]. The smaller entropy values  $S_M$  in the phase *IV* compared to the phases *II* and *III*, probably signal the larger noncollinearity of the magnetic structures in the latter states.

Our element-selective XMCD results complemented by this MCE data provide compelling evidence for the proposed noncollinear (collinear) magnetic structures in the phases *II* and *III* (*IV*). This is in line with a recent report suggesting a spin current or inverse Dzyaloshinskii-Moriya mechanism to be responsible for the multiferroic properties observed in the phases *II* and *III* [16]. Furthermore, our MCE results indicate the importance of the adiabatic temperature changes for mapping the  $H$ - $T$  phase diagram from pulsed-field experiments (see Sec. IV of the Supplemental Material [12]).

Remarkably, our observations signal the presence of a tetracritical point in the phase diagram, which was already suggested from the phase diagram determined from pyrocurrent measurements [16]. The transition lines that cross at the TP presumably belong to second-order transitions, because of the absence of any divergent and/or hysteretic behavior in the experimental results. Although thermodynamically controversial, the TP, where four second-order

transition lines meet, has been theoretically predicted [13, 14, 28, 29] for AFM systems with competing magnetic anisotropies, and experimentally observed as well [30, 31]. On the other hand,  $\text{MnCr}_2\text{S}_4$  has three spin degrees of freedom ( $n = 3$ ), dominated by rather isotropic Mn-Mn, Mn-Cr, and Cr-Cr Heisenberg exchange interactions. According to renormalization-group theory, the TP does not emerge in  $n = 3$  spin systems under uniform or staggered magnetic fields with either longitudinal or transverse component [14, 29]. In  $\text{MnCr}_2\text{S}_4$ , the intermediate phase (*III*) is stabilized via spin-lattice coupling (see Sec. V of the Supplemental Material [12]). Monte-Carlo calculations show that strong spin-lattice interaction in  $\text{MnCr}_2\text{S}_4$  spontaneously breaks the  $Z_2$  symmetry of the Mn-Cr bonds in the phases *III*, *IV*, and *V* [11] and effectively generates staggered magnetic fields at the site of the manganese spins. The effective staggered field in  $\text{MnCr}_2\text{S}_4$  has both longitudinal and transverse components with respect to the uniform external magnetic field, originating from a slight canting of the Cr moment observed in our experiments [Fig. 2(b)]. This stabilizes the asymmetric intermediate phase and results in the TP, which is rather unusual for conventional Heisenberg systems [29].

Finally, we discuss the symmetry of the phases *I*-*IV* based on the magnetic structures deduced from the current study. At zero field, with decreasing temperature, the  $O(3)$  and  $O(2)$  symmetries are successively broken at  $T_C$  and  $T_{\text{YK}}$ , respectively. In finite magnetic fields, the  $O(3)$  symmetry is always broken. In the low-field intermediate phase *III*, both the  $O(2)$  and  $Z_2$  symmetries are broken. On the other hand, in the plateau phase *IV*, the  $Z_2$  symmetry is kept broken, while the  $O(2)$  symmetry is restored. A series of symmetry breakings at the respective phase transitions is consistent with the earlier theoretical studies which predict the TP [14, 29].

In summary, element-specific XMCD together with the observed entropy variations provide direct evidence of the proposed noncollinear magnetic structures in the YK (*II*), low-field asymmetric (*III*), and plateau (*IV*) phases. Because the  $H$ - $T$  phase diagram of  $\text{MnCr}_2\text{S}_4$  is symmetric with respect to a field of approximately 40 T [11, 15], the present results provide a plausible description of the magnetic structures beyond 40 T, in phase *V*, and the higher-field phase (called inverse YK phase in Ref. [11]) close to saturation. In addition, our thermodynamic results hint toward an alternative route to the tetracritical point (TP) due to significant spin-lattice couplings in frustrated systems. We believe the understanding of the relation between the TP and spin-strain interactions might give further insight into the spin-superfluid and supersolid states suggested in analogy to bosonic systems [15, 32].

We acknowledge the support of the HLD at HZDR, member of the European Magnetic Field Laboratory (EMFL), the Deutsche Forschungsgemeinschaft



(DFG) through SFB 1143, the Würzburg-Dresden Cluster of Excellence on Complexity and Topology in Quantum Matter–*ct.qmat* (EXC 2147, Project ID 390858490), and the BMBF via DAAD (Project ID 57457940). This work was partly supported by the DFG through Transregional Research Collaboration TRR 80 (Augsburg, Munich, and Stuttgart) as well as by the project ANCD 20.80009.5007.19 (Moldova). This work was partly performed at High Field Laboratory for Superconducting Materials, Institute for Materials Research, Tohoku University (Project No 19H0505). The synchrotron radiation experiments were performed at the BL25SU of SPring-8 with the approval of the Japan Synchrotron Radiation Research Institute (JASRI) (Proposal No. 2019A1534, 2019B1474). We would like to thank A. Miyata for fruitful discussions and P. T. Cong for technical support.

---

\* Electronic address: s.yamamoto@hzdr.de

- [1] C. Lacroix, P. Mendels, and F. Mila, *Introduction to Frustrated Magnetism* (Springer, Berlin, Heidelberg, 2011).
- [2] S. A. Zvyagin, D. Graf, T. Sakurai, S. Kimura, H. Nojiri, J. Wosnitza, H. Ohta, T. Ono, and H. Tanaka, Pressure-tuning the quantum spin Hamiltonian of the triangular lattice antiferromagnet  $\text{Cs}_2\text{CuCl}_4$ , *Nat. Commun.* **10**, 1064 (2019).
- [3] B. Willenberg *et al.*, Magnetic frustration in a quantum spin chain: The case of linarite  $\text{PbCuSO}_4(\text{OH})_2$ , *Phys. Rev. Lett.* **108**, 117202 (2012).
- [4] H. T. Diep *et al.*, *Frustrated Spin Systems* (World Scientific, Singapore, 2013).
- [5] H. Kawamura, Universality of phase transitions of frustrated antiferromagnets, *J. Phys.: Condens. Matter* **10**, 4707 (1998).
- [6] T. Rudolf, Ch. Kant, F. Mayr, J. Hemberger, V. Tsurkan, and A. Loidl, Spin-phonon coupling in antiferromagnetic chromium spinels, *New J. Phys.* **9**, 76 (2007).
- [7] V. Tsurkan, S. Zherlitsyn, S. Yasin, V. Felea, Y. Skourski, J. Deisenhofer, H. -A. Krug von Nidda, J. Wosnitza, and A. Loidl, Unconventional magnetostructural transition in  $\text{CoCr}_2\text{O}_4$  at high magnetic fields, *Phys. Rev. Lett.* **110**, 115502 (2013).
- [8] J. Wosnitza, S. A. Zvyagin, and S. Zherlitsyn, Frustrated magnets in high magnetic fields: selected examples, *Rep. Prog. Phys.* **79**, 074504 (2016).
- [9] V. Tsurkan *et al.*, Magnetic, heat capacity, and conductivity studies of ferrimagnetic  $\text{MnCr}_2\text{S}_4$  single crystals, *Phys. Rev. B*, **68**, 134434 (2003).
- [10] P. K. Baltzer, P. J. Wojtowicz, M. Robbins, and E. Lopatin, Exchange interactions in ferromagnetic chromium chalcogenide spinels, *Phys. Rev.* **151**, 367 (1966).
- [11] A. Miyata *et al.*, Spin-lattice coupling in a ferrimagnetic spinel: Exotic  $H$ - $T$  phase diagram of  $\text{MnCr}_2\text{S}_4$  up to 110 T, *Phys. Rev. B* **101**, 054432 (2020).
- [12] See Supplemental Material at xxx for the predicted magnetic structures in magnetic-field-induced phases, experimental details, ultrasound and specific-heat results, MCE effects on the  $H$ - $T$  phase diagram, and spin-lattice coupling model, which includes Refs. [9, 11, 15, 16, 24, 33–40].
- [13] K.-S. Liu and M. E. Fisher, Quantum Lattice Gas and the Existence of a Supersolid, *J. Low Temp. Phys.* **10**, 655 (1973).
- [14] M. E. Fisher and D. R. Nelson, Spin Flop, Supersolids, and Bicritical and Tetracritical Points, *Phys. Rev. Lett.* **32**, 1350 (1974).
- [15] V. Tsurkan, S. Zherlitsyn, L. Prodan, V. Felea, P. T. Cong, Y. Skourski, Z. Wang, J. Deisenhofer, H.-A. Krug von Nidda, J. Wosnitza, and A. Loidl, Ultra-robust high-field magnetization plateau and super-solidity in bond-frustrated  $\text{MnCr}_2\text{S}_4$ , *Sci. Adv.* **3**, e1601982 (2017).
- [16] A. Ruff, Z. Wang, S. Zherlitsyn, J. Wosnitza, S. Krohns, H.-A. Krug von Nidda, P. Lunkenheimer, V. Tsurkan, and A. Loidl, Multiferroic spin-superfluid and spin-supersolid phases in  $\text{MnCr}_2\text{S}_4$ , *Phys. Rev. B* **100**, 014404 (2019).
- [17] J. X. Wang, L. Lin, C. Zhang, H. F. Guo, and J. -M. Liu, Experimental observation of ferroelectricity in ferrimagnet  $\text{MnCr}_2\text{S}_4$ , *Appl. Phys. Lett.* **117**, 032903 (2020).
- [18] M. Matsuda, H. Ueda, A. Kikkawa, Y. Tanaka, K. Katsumata, Y. Narumi, T. Inami, Y. Ueda, and S. -H. Lee, Spin-lattice instability to a fractional magnetization state in the spinel  $\text{HgCr}_2\text{O}_4$ , *Nat. Phys.* **3**, 397 (2007).
- [19] A. Miyata, H. Ueda, Y. Ueda, H. Sawabe, and S. Takeyama, Magnetic phases of a highly frustrated magnet,  $\text{ZnCr}_2\text{O}_4$ , up to an ultrahigh magnetic field of 600 T, *Phys. Rev. Lett.* **107**, 207203 (2011).
- [20] V. Tsurkan, M. Mücksch, H.-A. Krug von Nidda, J. Hemberger, D. Samusi, A. Loidl, S. Horn, and R. Tidecks, Anomalous magneto-crystalline anisotropy of  $\text{MnCr}_2\text{S}_4$  single crystals, *Solid State Commun.* **123**, 327 (2002).
- [21] J. I. Hwang *et al.*, X-ray magnetic circular dichroism characterization of  $\text{GaN}/\text{Ga}_{1-x}\text{Mn}_x\text{N}$  digital ferromagnetic heterostructure, *Appl. Phys. Lett.* **91**, 072507 (2007).
- [22] A. Kimura, J. Matsuno, J. Okabayashi, A. Fujimori, T. Shishidou, E. Kulatov, and T. Kanomata, Soft x-ray magnetic circular dichroism study of the ferromagnetic spinel-type Cr chalcogenides, *Phys. Rev. B* **63**, 224420 (2001).
- [23] A. Deb, M. Mizumaki, T. Muro, Y. Sakurai, and V. Tsurkan, Soft-x-ray magnetic-circular-dichroism study of the colossal-magnetoresistance spinel  $\text{Fe}_{0.5}\text{Cu}_{0.5}\text{Cr}_2\text{S}_4$ , *Phys. Rev. B* **68**, 014427 (2003).
- [24] Sh. Yamamoto, D. I. Gorbunov, H. Akai, H. Yasumura, Y. Kotani, T. Nakamura, T. Kato, N. V. Mushnikov, A. V. Andreev, H. Nojiri, and J. Wosnitza, Element- and orbital-selective magnetic coherent rotation at the first-order phase transition of a hard uniaxial ferrimagnet, *Phys. Rev. B* **101**, 174430 (2020).
- [25] G. van der Laan, and A. I. Figueroa, X-ray magnetic circular dichroism – a versatile tool to study magnetism, *Coord. Chem. Rev.* **277**, 95 (2014).
- [26] J. Denis, Y. Allain, and R. Plumier, Magnetic behavior of  $\text{MnCr}_2\text{S}_4$  in high magnetic fields, *J. Appl. Phys.* **41**, 1091 (1970).
- [27] R. Plumier, The magnetic structure of sulfur spinel  $\text{MnCr}_2\text{S}_4$  under applied magnetic field, *J. Phys. Chem. Solids* **41**, 871 (1980).
- [28] A. D. Bruce, and A. Aharony, Coupled order param-

- ters, symmetry-breaking irrelevant scaling fields, and tetracritical points, Phys. Rev. B **11**, 478 (1975).
- [29] J. M. Kosterlitz, D. R. Nelson, and M. E. Fisher, Bicritical and tetracritical points in anisotropic antiferromagnetic systems, Phys. Rev. B **13**, 412 (1976).
  - [30] L. Bevaart, E. Frikkee, and L. J. de Jongh, Neutron-scattering study of magnetic-field-induced transitions in a two-component antiferromagnetic system with competing spin anisotropies, Phys. Rev. B **19**, 4741 (1979).
  - [31] Y. Shapira, Tetracriticality of  $\text{RbMnF}_3$ , J. Appl. Phys. **52**, 1926 (1981).
  - [32] H. Matsuda, and T. Tsuneto, Off-diagonal long-range order in solids, Prog. Theor. Phys. Supp. **46**, 411 (1970).
  - [33] Y. Senba *et al.*, Upgrade of beamline BL25SU for soft x-ray imaging and spectroscopy of solid using nano- and micro-focused beams at SPring-8, AIP Conf. Proc. **1741**, 030044 (2016).
  - [34] T. Nakamura *et al.*, Soft X-ray magnetic circular dichroism of a  $\text{CoFe/MnIr}$  exchange bias film under pulsed high magnetic field, Appl. Phys. Express **4**, 066602 (2011).
  - [35] S. Zherlitsyn, S. Yasin, J. Wosnitza, A. A. Zvyagin, A. V. Andreev, and V. Tsurkan, Spin-lattice effects in selected antiferromagnetic materials, Low Temp. Phys. **40**, 123 (2014).
  - [36] S. Riegel, and G. Weber, A dual-slope method for specific heat measurements, J. Phys. E **19**, 790 (1986).
  - [37] T. Kihara, Y. Kohama, Y. Hashimoto, S. Katsumoto, and M. Tokunaga, Adiabatic measurements of magneto-caloric effects in pulsed high magnetic fields up to 55 T, Rev. Sci. Instrum. **84**, 074901 (2013).
  - [38] T. Nomura, Y. Kohama, Y. H. Matsuda, K. Kindo, and T. C. Kobayashi,  $\alpha$ - $\beta$  and  $\beta$ - $\gamma$  phase boundaries of solid oxygen observed by adiabatic magnetocaloric effect, Phys. Rev. B **95**, 104420 (2017).
  - [39] Y. Skourski, M. D. Kuz'min, K. P. Skokov, A. V. Andreev, and J. Wosnitza, High-field magnetization of  $\text{Ho}_2\text{Fe}_{17}$ , Phys. Rev. B **83**, 214420 (2011).
  - [40] J. Brambleby *et al.*, Adiabatic physics of an exchange-coupled spin-dimer system: Magnetocaloric effect, zero-point fluctuations, and possible two-dimensional universal behavior, Phys. Rev. B **95**, 024404 (2017).